Nano Energy 38 (2017) 51–58

Contents lists available at ScienceDirect

Nano Energy

journal homepage: www.elsevier.com/locate/nanoen

Full paper

High efficiency perovskite light-emitting diodes of ligand-engineered colloidal formamidinium lead bromide nanoparticles

Young-Hoon Kim[a,b,c,1], Geon-Hui Lee[d,1], Young-Tae Kim[d], Christoph Wolf[d], Hyung Joong Yun[e], Woosung Kwon[f], Chan Gyung Park[d], T.-W Lee[a,b,c,*]

[a] Department of Materials Science and Engineering, Seoul National University, 1 Gwanak-ro, Gwanak-gu, Seoul 08826, Republic of Korea
[b] Research Institute of Advanced Materials, Seoul National University, 1 Gwanak-ro, Gwanak-gu, Seoul 08826, Republic of Korea
[c] BK21 PLUS SNU Materials Division for Educating Creative Global Leaders, Seoul National University, 1 Gwanak-ro , Gwanak-gu, Seoul 08826, Republic of Korea
[d] Department of Materials Science and Engineering, Pohang University of Science and Technology (POSTECH), Pohang, Gyungbuk 790-784, Republic of Korea
[e] Advance Nano Research Group, Korea Basic Science Institute (KBSI), 169-148 Gwahak-ro, Daejeon 34133, Republic of Korea
[f] Department of Chemical and Biological Engineering, Sookmyung Women's University, 100 Cheongpa-ro 47-gil, Yongsan-gu, Seoul 04310, Republic of Korea

ARTICLE INFO

Keywords:
Formamidinium lead bromide
Nanoparticle
Light-emitting diodes
Charge injection
Luminescence efficiency

ABSTRACT

Formamidinium (FA, $CH(NH_2)_2$) lead bromide perovskite ($FAPbBr_3$) nanoparticles (NPs) are promising emitters due to their high stability and ability to emit pure green color in both film and solution states. Even though various types of metal halide NP emitters in solution have shown high photoluminescence quantum efficiencies (PLQEs), electroluminescence efficiencies of the light-emitting diodes (LEDs) using the NP films are still much poorer, possibly due to the insulating ligands which can impede the charge injection and transport in films. Therefore, the organic ligand of NPs should be designed to facilitate charge injection and transport in LEDs. Here, we synthesize ligand-engineered colloidal $FAPbBr_3$ NPs at RT and demonstrate high efficiency perovskite NP LEDs based on the $FAPbBr_3$ NPs. Control of ligand length reduces trap-assisted recombination of carriers at the surface traps, and thus maximizes the PLQE of $FAPbBr_3$ NPs. Ligand engineering can also improve the charge injection and transport capability in $FAPbBr_3$ NP films. With this ligand engineering method, we achieve maximum current efficiency of 9.16 cd/A in LEDs based on $FAPbBr_3$ NPs, which is the highest efficiency in $FAPbBr_3$ NP-LEDs to date. The ligand engineering method reported here can be a simple way to improve the luminescence efficiency of optoelectronic devices based on perovskite NP LEDs.

1. Introduction

Organic-inorganic hybrid perovskite (OIP) materials are promising emitters due to widely-tunable emission wavelength (400 nm≤λ≤780 nm), high color purity with narrow full width at half maximum ((FWHM) ~ 20 nm) and low material cost [1–10]. Furthermore, their solution-processability as polycrystalline bulk films has allowed a rapid increase in electroluminescence (EL) efficiency from 0.1% of exterial quantum efficiency *EQE* to 11.7% in only three years by reducing perovskite grain size or by incorporating various organic ammonium moieties in their crystals [1–10]. Nevertheless, polycrystalline bulk films of OIPs still need to overcome low photoluminescence quantum efficiency (PLQE) at low excitation density ($< 10^{20}$ cm^{-3}), and low EL efficiency at low current density, due to low radiative recombination rate of electron-hole pairs under these conditions [1–7,11].

Colloidal OIP nanoparticles (NPs) can be another form of OIP emitters that can achieve high EL efficiency by efficiently confining the exciton in perovskite NPs (≤20 nm) [1,11]. Recently, bright-green-emitting colloidal OIP-NPs based on methylammonium (MA, CH_3NH_3) lead bromide ($CH_3NH_3PbBr_3$) have been demonstrated and high PLQE (~90%) have been achieved [11,12]. Furthermore, their simple synthesis process at room temperature (RT) showed great possibility for wide use in industry [11,12]. However, EL device made of the colloidal $MAPbBr_3$-NPs still showed much poorer EL efficiencies (current efficiency *CE*~11.49 cd/A and *EQE*~3.8%) [13] than did $MAPbBr_3$ polycrystalline bulk film-based light-emitting diodes (LEDs) (*CE*~42.9 cd/A and *EQE*~8.53%) [2] possibly due to inefficient charge injection and transport though the insulating ligand. Furthermore, MA cation can reduce the stability of the perovskite crystal under heat, moisture and light [14], so $MAPbBr_3$-based colloidal perovskite NPs are not sufficiently stable.

* Corresponding author.
E-mail addresses: twlees@snu.ac.kr, taewlees@gmail.com (T.-W. Lee).
[1] These authors contributed equally to this work.

http://dx.doi.org/10.1016/j.nanoen.2017.05.002
Received 31 March 2017; Received in revised form 29 April 2017; Accepted 1 May 2017
Available online 05 May 2017

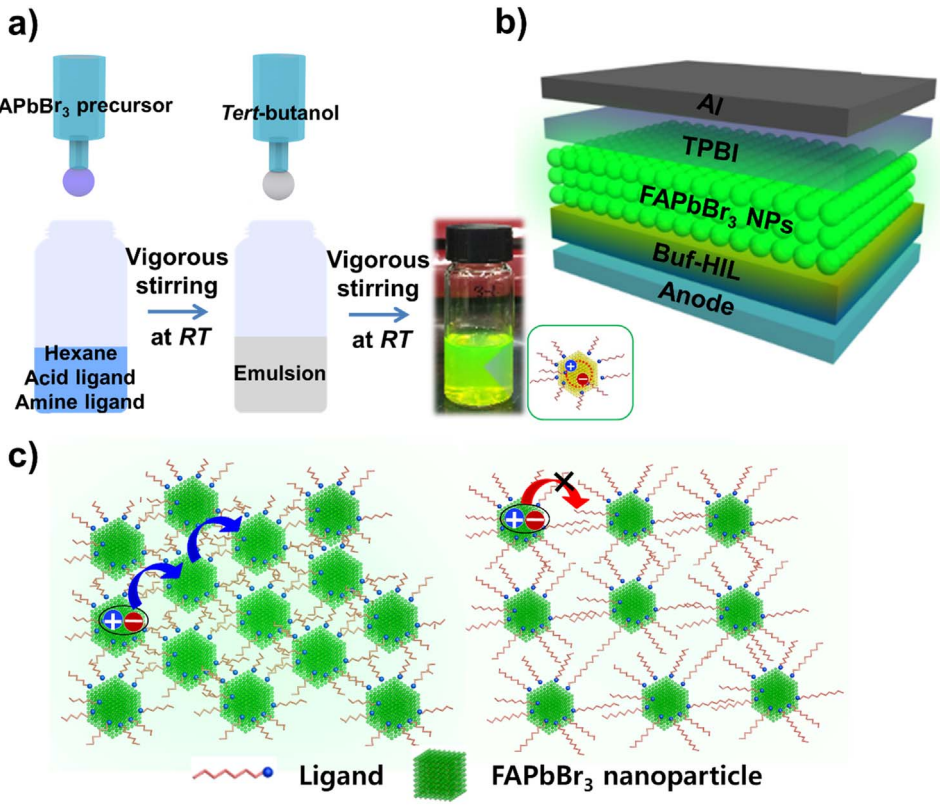

Fig. 1. a) Synthesis schematic of $FAPbBr_3$ NPs using emulsion system at room temperature, b) device architecture of $FAPbBr_3$ NP-LEDs, c) schematic illustration of luminescence efficiency and charge injection/transport capabilities in $FAPbBr_3$ NP films with short ligand (left) and long ligand (right). Blue arrows: permitted transitions; red arrow: impeded transitions.

All-inorganic perovskite (AIP) NPs ($CsPbBr_3$) can overcome the low stability of $MAPbBr_3$-based green-emitting OIP-NPs owing to higher thermal decomposition temperature (~580 °C) of $CsPbBr_3$ than that of $MAPbBr_3$ (~220 °C) [15–18]. However, green-emitting $CsPbBr_3$ NPs cannot fully match the pure green color (~520 nm) in the National Television System Committee (NTSC) chromaticity diagram because their photoluminescence (PL) spectrum is located below 520 nm, even for the NPs with larger size than exciton Bohr diameter (> 10 nm) [19]. Green-emitting AIP-NPs can emit PL > 520 nm and fulfill the pure green color by incorporating mixed halide ($CsPbBr_3I_{3-x}$), but they showed reduced PLQE [20,21].

Formamidinium (FA, $CH(NH_2)_2$) lead bromide ($CH(NH_2)_2PbBr_3$) based colloidal OIP-NPs can be a favorable way to improve the stability of perovskite crystal and fulfill the pure green color (PL spectra≥520 nm) in the NTSC chromaticity diagram [22–25]. FA has strong ionic interaction with halogen anions (Br^-) in the perovskite crystal due to its larger size than MA, and thus $FAPbBr_3$ shows higher chemical stability than $MAPbBr_3$ [22–25]. $FAPbBr_3$ NPs can also maintain the bright PL emission in film states and under the high temperature [25]. Furthermore, the large size of FA in $FAPbBr_3$ NPs reduces the band gap compared to that of $CsPbBr_3$ NPs, and therefore induced a PL spectrum≥520 nm that can fulfill the pure green color in the NTSC chromaticity diagram [25]. However, compared to the $MAPbBr_3$ NPs and $CsPbBr_3$ NPs, only little research based on synthesis of colloidal $FAPbBr_3$ NPs and applications on LEDs has been reported [25,26].

Recently, colloidal $FAPbBr_3$ NPs synthesized at RT and their application in LEDs were demonstrated, and achieved maximum *CE*~6.4 cd/A [26]. Charge injection and transport in $FAPbBr_3$ NP films relies on the length of the insulating hydrocarbon chain in organic ligands, so these processes in devices can be inefficient in the devices [26–28]. Therefore, organic ligands should be controlled to facilitate the charge injection and transport in $FAPbBr_3$ NP film devices. Here, we synthesized colloidal $FAPbBr_3$ NPs at RT and demonstrated high-efficiency LEDs (Fig. 1a,b). We boosted the EL efficiency of colloidal $FAPbBr_3$ NPs by i) maximizing the PLQE of NPs, and ii) improving the charge injection and transport capability in NP films by controlling the length of hydrocarbon chain in the amine ligand. This ligand length control can maximize the PLQE of $FAPbBr_3$ NPs because the size, which strongly affects the trap density on the surface of NPs, can be controlled by the ligand length [29–32]. The charge injection and transport capability in NP films can be also dramatically improved by reducing the ligand length, because the hydrocarbon chain in organic ligands is an insulator and therefore impedes charge injection and transport in NP films (Fig. 1c) [27–30]. However, when the ligand is too short, the $FAPbBr_3$ NPs can be unstable, so luminescence efficiencies dramatically decrease. With these strategies, we achieved maximum *CE* of 9.16 cd/A in $FAPbBr_3$ NP based LEDs, which is the highest value in $FAPbBr_3$ NP LEDs to date. This result verifies that control of the ligand length in $FAPbBr_3$ NPs is a simple and primary way to improve the device efficiency. Furthermore, we investigated the origin of high luminescence efficiency in LEDs by analyzing temperature-dependent PL, PLQE, time-correlated single photon counting (TCSPC), and hole-only and electron-only current density data.

2. Experimental section

2.1. Synthesis of perovskite nanoparticles

We dissolved 0.4 mmol of $CH(NH_2)_2Br$ (Sigma-Aldrich) and 0.4 mmol of $PbBr_2$ (Dyesol) in 1 mL of DMF to form a precursor solution. In another vial, we mixed 6.05 μmol of amine ligand and 0.25 mL of oleic acid with 5 mL of hexane. Dropping 0.4 mL of precursor solution into ligand-dissolved hexane solution with vigorous stirring yielded a milky emulsion. Dropwise addition of 4 mL of *tert*-butanol into the emulsion solution caused crystallization of perovskite

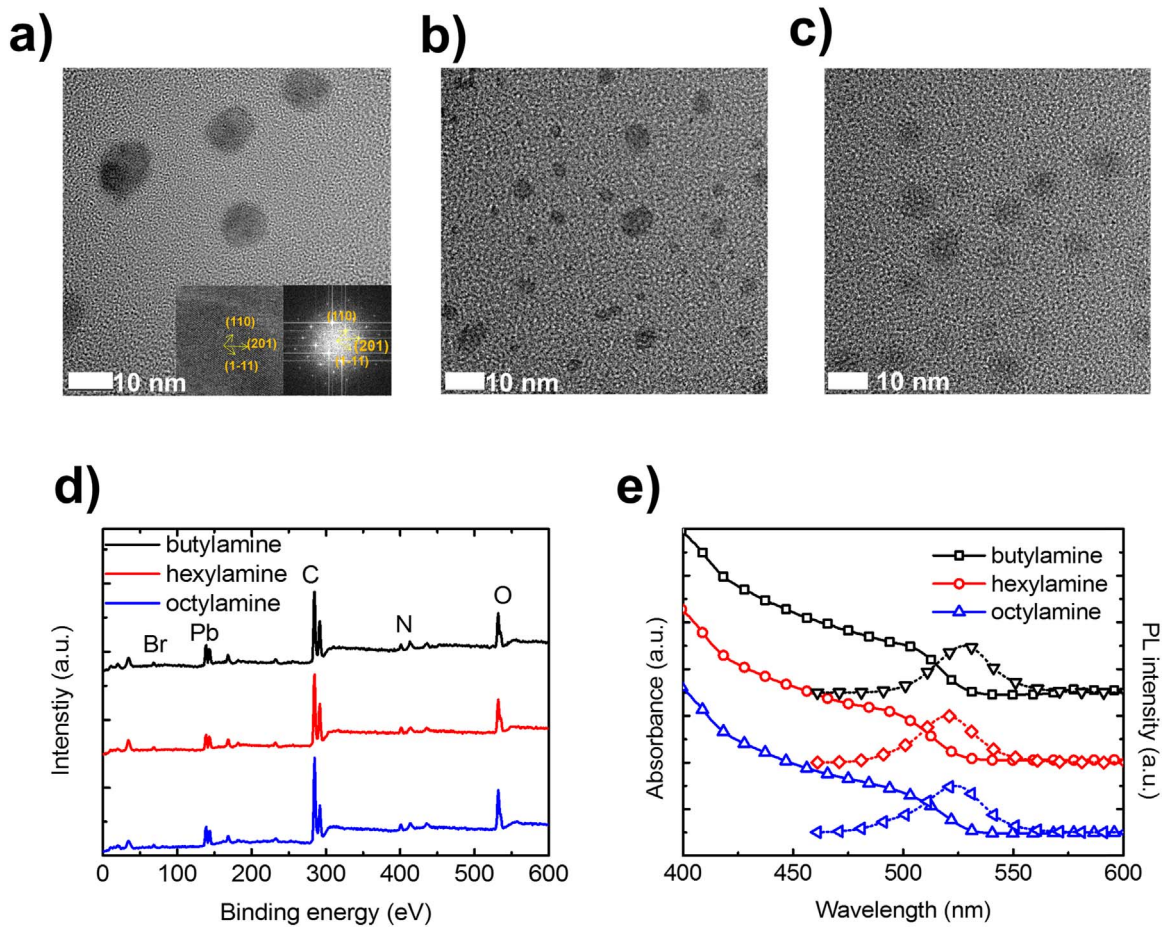

Fig. 2. a) TEM image, high-resolution TEM image and fast Fourier Transform pattern (inset) of $FAPbBr_3$ NPs with butylamine, b) TEM image of $FAPbBr_3$ NPs with hexylamine, c) TEM image of $FAPbBr_3$ NPs with octylamine, d) XPS survey of $FAPbBr_3$ NPs with various amine ligands and e) PL spectra and UV/Vis absorption spectra of $FAPbBr_3$ NPs with various amine ligands.

precursor, and the milky solution turned to yellow-green. The solution was centrifuged at 10,000 rpm for 10 min, then the bottom precipitate was discarded.

2.2. LED Fabrication and characterization

ITO patterned glasses were cleaned by sonication in acetone and 2-isopropanol for 15 min sequentially, and then boiled in 2-isopropanol for 30 min. The glasses were dried, then UV-ozone was treated for 10 min. After ozone treatment, Buf-HIL was spin-coated on the ITO patterned glasses at 4500 rpm for 90 s, then baked at 150 °C for 30 min. The substrates were transferred to a glove box and $FAPbBr_3$ NP solutions were spin-coated at 3000 rpm for 90 s. They were then baked at 90 °C for 10 min, then loaded in a vacuum chamber (< 10^7 Torr). Then, TPBI (50 nm) was deposited at 1 Å/s, LiF (1 nm) was deposited at 0.1 Å/s, and Al (100 nm) was deposited at 3 Å/s sequentially. The current-voltage-luminance were measured using a Minolta CS2000 spectro-radiometer and Keithley 2400 source meter.

2.3. Time-correlated single photon counting measurement

A picosecond-pulse laser head (LDH-P-C-405B, PicoQuant) with 405-nm excitation wavelength and 40-MHz repetition rate was used as an excitation source. The emitted light was resolved and detected by monochromator (SP-2155, Acton) and TCSPC module (PicoHarp, PicoQuant) with MCP-PMT (R3809U-50, Hamamatsu), respectively.

2.4. Photoluminescence (PL) and photoluminescence quantum efficiency (PLQE) measurement

PL spectra and PL matrix were measured using a spectrofluorometer (JASCO FP-8300). PLQEs of $FAPbBr_3$ NP solutions were measured using the same spectrofluorometer with a 100-nm integrating sphere (ILF-835) and Jasco SpectraManager II Software. The excitation wavelength for measuring PLQEs was 375 nm.

2.5. Transmission electron microscopy measurement

Transmission electron microscopy (TEM) experiment was conducted at an acceleration voltage of 200 kV using a JEOL-JEM 2100F.

2.6. Ultraviolet photoelectron spectroscopy (UPS) and X-ray photoelectron spectroscopy (XPS) measurement

UPS and XPS of $FAPbBr_3$ NPs in form of films (glass/ITO/Buf-HIL/NP films) were measured by using the same photoelectron spectrometer (Kratos Inc., AXIS-UltraDLD) at the Korea Basic Science Institute.

3. Results and discussion

We developed an emulsion system that uses two immiscible solvents (*n,n*-dimethylformamidinium (DMF) and hexane) to synthesize the efficient $FAPbBr_3$ NPs (Fig. 1a). We dropped the perovskite precursor solution dissolved in DMF into a mixture of oleic acid

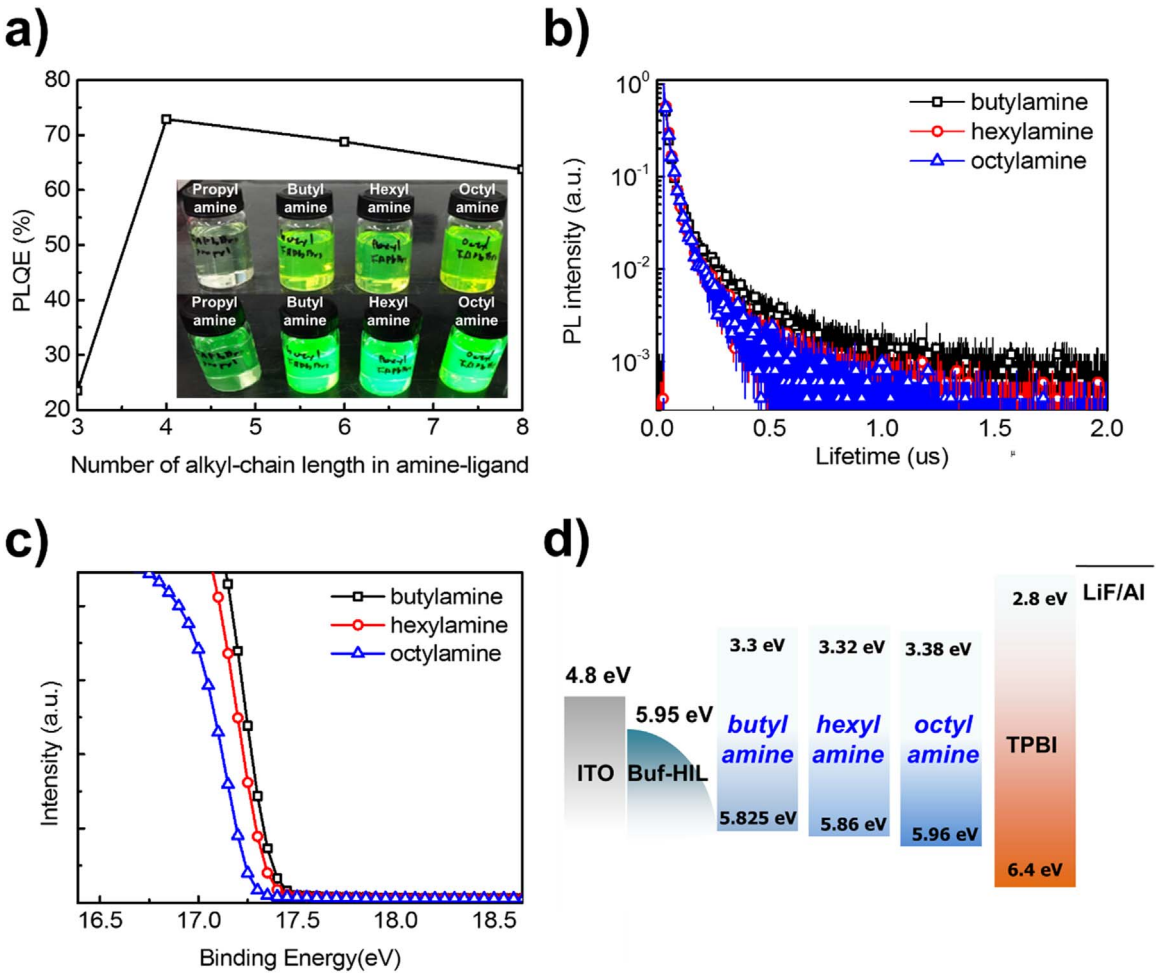

Fig. 3. a) PLQE and photograph under ambient light and under λ=350 nm Xe lamp (inset) of $FAPbBr_3$ NPs with various amine ligands, b) PL lifetime curves of $FAPbBr_3$ NPs with various amine ligands, c) secondary cut-off of $FAPbBr_3$ NPs with various amine ligands obtained by UPS, d) energy band diagram of $FAPbBr_3$ NP-LEDs.

Table 1
Lifetime τ_1 and fraction f_1 of trap-assisted recombination of carriers at the surface of $FAPbBr_3$ NPs, lifetime τ_2 and fraction f_2 of recombination of geminate electron-hole pairs inside the NPs, and average lifetime τ_{avg} of $FAPbBr_3$ NPs.

Amine ligand	τ_1 (ns)	f_1 (%)	τ_2 (ns)	f_2 (%)	τ_{avg} (ns)
butylamine	22.93	56.72	154	43.28	79.63
hexylamine	20.57	63.5	102.54	36.5	50.5
octylamine	20.87	64.32	102.52	35.68	50

($C_{17}H_{33}COOH$), amine ligands (*n*-butylamine ($C_4N_9NH_2$) or *n*-hexylamine ($C_6N_{13}NH_2$) or *n*-octylamine ($C_8N_{17}NH_2$)) and hexane to introduce the emulsion solution. When demulsifier (*tert*-butanol) was dropped into the emulsion solution, the two immiscible solvents mixed with each other and the perovskite precursor was crystallized [33]. Oleic acid improves the stability of crystallized perovskite NPs by suppressing their re-aggregation, and amine ligands prevent the formation of large crystals (> micrometer) by controlling the kinetics of crystallization [11,12].

$FAPbBr_3$ NPs synthesized using *n*-butylamine were circular with diameter d~10 nm, but those synthesized using *n*-hexylamine and *n*-octylamine had smaller diameter (d < 10 nm) (Fig. 2a-c and Fig. S1). We attribute this decrease of NP size with increasing ligand length to the suppression of perovskite crystal growth under the long ligand [29,30]. However, similar dimension of $FAPbBr_3$ NPs with *n*-hexylamine and those with *n*-octylamine were possibly due to the saturation of suppression effect of amine ligand on the perovskite crystal growth when we used amine ligand longer than *n*-hexylamine. High-resolution transmission electron microscopy (HR-TEM) and fast Fourier Transform (FFT) showed clear cubic $Pm\bar{3}m$ crystals with inter-planar distances of 4.1 Å, 3.781 Å and 2.633 Å, which correspond to (110), (1$\bar{1}$1) and (201), respectively (Inset in Fig. 2a) [26].

X-ray photoelectron spectroscopy (XPS) and Fourier-transform infrared (FT-IR) spectroscopy showed the chemical characteristics of $FAPbBr_3$ NPs. All $FAPbBr_3$ NPs showed XPS peaks corresponding to C (~ 285 eV), N (~400 eV), Br (~68 eV), Pb (~138 and 143 eV) and O (~533 eV) which indicated the presence of oleic acid, amine ligand and $FAPbBr_3$ perovskite crystal in NP films (Fig. 2d and Figs. S2-4). In all FT-IR data, we can also clearly find the C-O bend (1200–1300 cm^{-1}) and C=O stretch (1700–1750 cm^{-1}) which confirmed the oleic acid, and C-N stretches (1020–1200 cm^{-1}), N-H bend (1590–1650 cm^{-1}), C-H stretches (2850–3000 cm^{-1}) and N-H stretches (3000–3300 cm^{-1}) that indicated the presence of $FAPbBr_3$ perovskite crystals and amine ligand, respectively (Fig. S5).

Absorption onset occurred at ~520 nm in all $FAPbBr_3$ NPs. $FAPbBr_3$ NPs with *n*-butylamine had PL peak at ~528 nm with high color purity (FWHM ~27 nm) (Fig. 2e). Because of smaller particle size of $FAPbBr_3$ NPs with *n*-hexylamine and *n*-octylamine than the NPs with *n*-butylamine, they showed slightly blue-shifted PL peaks at ~522 nm due to quantum confinement [34]. Similar PL peak positions of $FAPbBr_3$ NPs with *n*-hexylamine and *n*-octylamine (~522 nm) also confirmed that suppression effect of amine ligand on the perovskite crystal growth was saturated and thus similar level of quantum confinement effect in $FAPbBr_3$ NPs occured when we used ligand

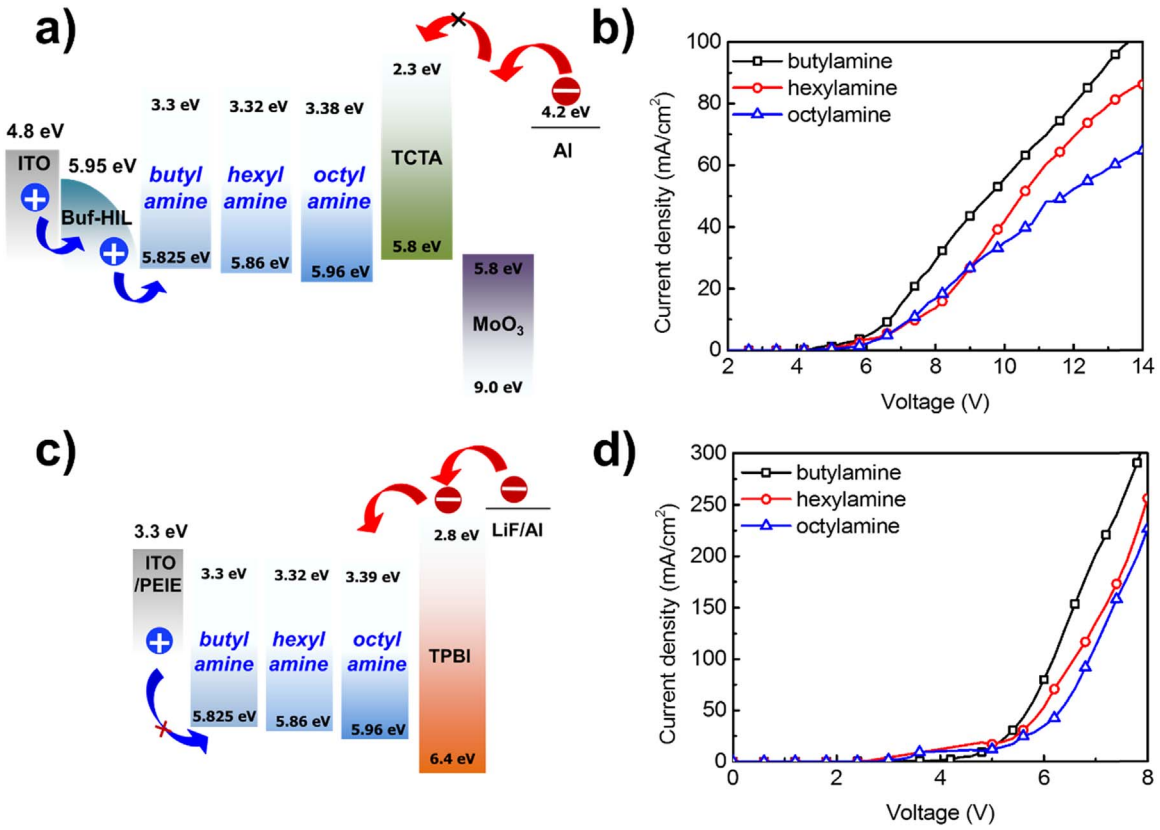

Fig. 4. a) Energy band diagram of hole-only devices (Blue arrows: permitted injections; red arrow: impeded injections), b) hole current density measured from hole-only devices, c) energy band diagram of electron-only devices (Blue arrows: impeded injections; red arrow: permitted injections) and d) electron current density measured from electron-only devices.

longer than *n*-hexylamine. These PL peaks of $FAPbBr_3$ NPs had λ≥520 nm, and therefore can satisfy the pure green color in the NTSC chromaticity diagram [25]. The Commission Internationale de l'Éclairage (CIE) coordinates of PL spectrum of $FAPbBr_3$ NPs were (0.171, 0.758) for NPs with *n*-butylamine, (0.126, 0.724) for NPs with *n*-hexylamine, and (0.135, 0.718) for NPs with *n*-octylamine, respectively (Fig. S6). These $FAPbBr_3$ NPs also showed constant PL peak position irrespective of the excitation wavelength; this consistency indicates that $FAPbBr_3$ NPs have pure $FAPbBr_3$ emitting centers without any others such as chromophores in ligands (Fig. S7).

$FAPbBr_3$ NPs with *n*-butylamine showed very high PLQE of ~72% which is attributed to the improved radiative recombination of charge carriers by efficient exciton confinement and increased exciton binding energy E_b in small perovskite NPs (Fig. 3a) [11]. The increased E_b of $FAPbBr_3$ NPs (> 140 meV) compared to polycrystalline bulk $FAPbBr_3$ film (≤25 meV) can be confirmed by measuring temperature-dependent PL intensities (Fig. S8) [35,36]. PLQE of $FAPbBr_3$ NPs gradually decreased with increasing amine ligand length from ~69% for NPs with *n*-hexylamine to ~64% for NPs with *n*-octylamine. We attribute this decrease to the increasing surface-to-volume ratio that results from reduced NP size and steric effect of long amine ligands which prevent them from fully passivating the NP surfaces; these induce the trap-assisted recombination of charge carriers at the surface traps [4,11,12,31,32,37]. However, $FAPbBr_3$ NPs with *n*-propylamine ($C_3N_7NH_2$) showed much decreased PLQE (~25%) because alkyl length in surface ligands is too short, and thus reduces the stability of NPs in solution. $FAPbBr_3$ NPs with *n*-propylamine also showed weak green color under ambient light and weak green emission under UV illumination, however, NPs with *n*-butylamine, *n*-hexylamine and *n*-octylamine showed the bright green emission under ambient light and UV illumination, respectively (Inset in Fig. 3a). To investigate the effect of ligand length in carboxylic acid, we used octanoic acid ($CH_3(CH_2)_6COOH$), which is shorter than oleic acid, and *n*-butylamine to synthesize the $FAPbBr_3$ NPs. $FAPbBr_3$ NPs with octanoic acid and *n*-butylamine showed dramatically reduced PLQE of ~24% because carboxylic acid with a short ligand length cannot suppress the re-aggregation of NPs, and thus reduces the stability of $FAPbBr_3$ NPs. Further research on synthesis of $FAPbBr_3$ NPs should be conducted to develop ways to control the ligand length of carboxylic acid to further improve the PLQE in $FAPbBr_3$ NPs and charge injection/transport capability in NP films.

To study the carrier dynamics in $FAPbBr_3$ NPs with different amine ligands, we conducted TCSPC. PL decay can be fitted by a double-exponential equation which indicates that PL decay occurs in a fast way and a slow way. The fast PL decay is related to the trap-assisted recombination of carriers at the surface traps of perovskite NPs; the slow PL decay is related to the recombination of geminate electron-hole pairs inside the NPs [4,19]. The $FAPbBr_3$ NPs showed shorter PL lifetime τ_{ave} than did polycrystalline bulk $FAPbBr_3$ films (> 200 ns) because the E_b increased (> 140 meV), so recombination of geminate electron-hole pairs mainly occured in their small NPs rather than free-carrier recombination [11,22–24]. Correspondingly, $FAPbBr_3$ NPs with longer ligand showed shorter τ_{ave} and higher fraction f_1 of fast PL decay (τ_{ave}~50.5 ns, f_1~63.5% for NPs with *n*-hexylamine; τ_{ave}~50 ns, f_1~64.3% for NPs with *n*-octylamine) than did those with shorter ligand (τ_{ave}~79.6 ns, f_1~56.7% for NPs with *n*-butylamine) (Fig. 3b, Table 1). These changes are attributed to the reduced size of $FAPbBr_3$ NPs and consequent increase in surface-to-volume ratio, which increased trap-assisted recombination of carriers at the surface traps, and thereby reduced the PLQE (Fig. 3a).

The band gap of $FAPbBr_3$ NPs can be calculated by considering the optical band gap measured by ultraviolet (UV)/visible absorption spectroscopy, E_b fitted by temperature-dependent PL, and ionization energy *IE* which can be calculated by adding the work function to the valence band edge obtained from ultraviolet photoelectron spectroscopy (UPS) (Figs. 2e, 3c and Figs. S8, S9). As amine ligand length

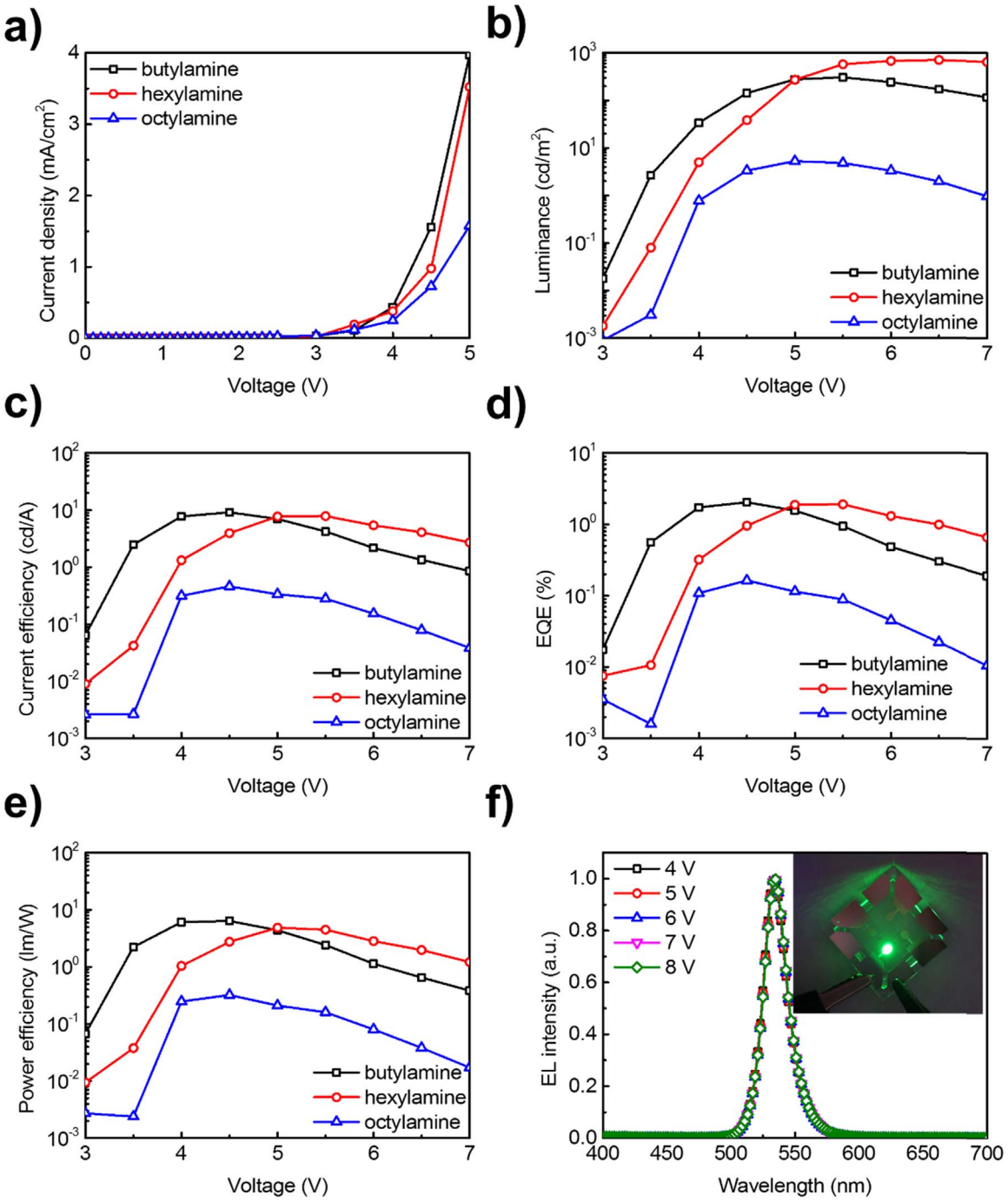

Fig. 5. a) Current density characteristics, b) luminance characteristics, c) *CE* characteristics, d) *EQE* characteristics, e) *PE* characteristics of $FAPbBr_3$ NP LED using various amine ligands and f) EL spectra at different applied bias and photograph (inset) of $FAPbBr_3$ NP LEDs using butylamine.

increased, the band gap and *IE* of $FAPbBr_3$ NPs gradually increase from 2.526 eV and 5.825 eV for NPs with *n*-butylamine to 2.58 eV and 5.96 eV for NPs with *n*-octylamine respectively, possibly due to the quantum-confinement effect under their decreasing NP size (Fig. 3d).

The charge injection and transport capabilities in $FAPbBr_3$ NP film also strongly affect the luminescence efficiency in NP-LEDs [27,28]. To characterize the charge injection and transport capabilities in NP films, we fabricated hole-only devices (ITO/Buffer hole injection layer (Buf-HIL) (~40 nm) [3,38–41]/$FAPbBr_3$ NP layer/Tris(4-carbazoyl-9-yl-phenyl)amine (~50 nm)/MoO_3 (~3 nm)/Al (~100 nm)) and electron-only devices (ITO/Polyethylenimine ethoxylated (~10 nm)/$FAPbBr_3$ NP layer/1,3,5-tris(N-phenylbenzimiazole-2-yl)benzene (TPBI) (~50 nm)/LiF (~1 nm)/Al (~100 nm)), and measured the hole current density and electron current density, respectively (Fig. 4). For both devices, current density obviously increased as ligand length decreased; these trends indicate that use of short amine ligand can increase the EL efficiency of $FAPbBr_3$ NPs by improving charge injection and transport capabilities in NP films as well as PLQE of NPs.

The device efficiencies were measured in simplified LEDs (ITO/Buf-HIL (~40 nm)/$FAPbBr_3$ NP layers/TPBI (~50 nm)/LiF/Al) using $FAPbBr_3$ NPs with various amine ligands. As the amine ligand length decreased, the current density of $FAPbBr_3$ NP LEDs gradually increased and turn-on voltage decreased, respectively (Fig. 5a,b and Table S1). These trends convincingly demonstrate that the insulating

hydrocarbon chain in organic ligands severely impedes charge injection and transport in $FAPbBr_3$ NP films; this result is consistent with the hole-only and electron-only current density (Fig. 4). As the ligand length decreased, $FAPbBr_3$ NP LEDs showed gradually increasing luminescence efficiencies from *CE*~0.46 cd/A, power efficiency *PE*~0.32 lm/W and *EQE*~0.164% for NPs with *n*-octylamine to *CE*~9.16 cd/A, *PE*~6.4 lm/W and *EQE*~2.05% for NPs with *n*-butylamine (Fig. 5c-e). Furthermore, in every applied bias, $FAPbBr_3$ NP LEDs showed gradually increasing luminance and *CE* as amine ligand length decreased (Table S2,3). These results were attributed to the enhanced formation of electron-hole pairs and thus their increased radiative decay due to improved balance between electron-hole injection/transport in $FAPbBr_3$ NP films by ligand engineering. These are to our best knowledge the highest luminescence efficiencies in LEDs with colloidal $FAPbBr_3$ NPs to date. These high device efficiencies can be attributed to the i) improved PLQE of $FAPbBr_3$ NPs due to reduced trap-assisted recombination of carriers at the surface traps, and ii) increased charge injection and transport capability in $FAPbBr_3$ NP films by control of the ligand length. $FAPbBr_3$ NP LEDs also showed very stable EL spectra under applied bias; this result indicates that $FAPbBr_3$ can emit the pure green light under the various electric fields (Fig. 5f and Fig. S10a,b). The EL spectra of $FAPbBr_3$ NPs (~530 nm) also exceed the wavelength ~520 nm and thus can fulfill the pure green color in the NTSC chromaticity diagram. The CIE coordinates of EL spectrum of $FAPbBr_3$ NPs were (0.223, 0.745) for NPs with *n*-butylamine, (0.180, 0.758) for NPs with *n*-hexylamine, and (0.202, 0.668) for NPs with *n*-octylamine, respectively; these are located outside of the NTSC standard colors (Fig. S10c).

4. Conclusion

We synthesized colloidal $FAPbBr_3$ NPs at RT whose ligand on the NP surface was controlled to boost up the efficiency of perovskite NP LEDs. Control of the ligand length improves the PLQE of emitters by reducing trap-assisted recombination of carriers, and facilitates charge injection and transport in $FAPbBr_3$ NP films. PLQE and TCSPC experiments confirmed the enhanced luminescence efficiency in NPs, and hole-only and electron-only current density characterizations verified the improved charge injection and transport capabilities in $FAPbBr_3$ NP films, respectively. This ligand engineering in $FAPbBr_3$ NPs achieved a maximum *CE* of 9.16 cd/A, *PE* of 6.4 lm/W and *EQE* of 2.05% in LEDs with pure green color in the NTSC chromaticity diagram, which is the highest efficiency to date among $FAPbBr_3$ NP-LEDs.

Our work suggests that molecular engineering of ligand on NPs can be a promising method to fabricate the high-efficiency $FAPbBr_3$ NP-LEDs that can fulfill the pure green color in the NTSC chromaticity diagram. Considering the low material cost and simple method to synthesize these emitters, which have high luminescence, and efficient charge injection/transport capabilities in film devices, our methods may enable the application of $FAPbBr_3$ NP emitters in next-generation displays and solid-state lighting.

Acknowledgements

This work was supported by the National Research Foundation of Korea (NRF) grant funded by the Korea government (Ministry of Science, ICT & Future Planning) (Grant No. NRF-2016R1A3B1908431).

Appendix A. Supplementary material

Supplementary data associated with this article can be found in the online version at doi:10.1016/j.nanoen.2017.05.002.

References

[1] Y.-H. Kim, H. Cho, T.-W. Lee, Proc. Natl. Acad. Sci. U. S. A. 113 (2016) 11694–11702.
[2] H. Cho, S.-H. Jeong, M.-H. Park, Y.-H. Kim, C. Wolf, C.-L. Lee, J.H. Heo, A. Sadhanala, N. Myoung, S. Yoo, S.H. Im, R.H. Friend, T.-W. Lee, Science 350 (2015) 1222–1226.
[3] Z.-K. Tan, R.S. Moghaddam, M.L. Lai, P. Docampo, R. Higler, F. Deschler, M. Price, A. Sadhanala, L.M. Pazos, D. Credgington, F. Hanusch, T. Bein, H.J. Snaith, R.H. Friend, Nat. Nanotechnol. 9 (2014) 687–692.
[4] Y.-H. Kim, H. Cho, J.H. Heo, T.-S. Kim, N. Myoung, C.-L. Lee, S.H. Im, T.-W. Lee, Adv. Mater. 27 (2015) 1248–1254.
[5] J. Byun, H. Cho, C. Wolf, M. Jang, A. Sadhanala, R.H. Friend, H. Yang, T.-W. Lee, Adv. Mater. 28 (2016) 7515–7520.
[6] Y.-K. Chih, J.-C. Wang, R.-T. Yang, C.-C. Liu, Y.-C. Chang, Y.-S. Fu, W.-C. Lai, P. Chen, T.-C. Wen, Y.-C. Huang, C.-S. Tsao, T.-F. Guo, Adv. Mater. 28 (2016) 8687–8694.
[7] J.C. Yu, D.W. Kim, D.B. Kim, E.D. Jung, J.H. Park, A.-Y. Lee, B.R. Lee, D.D. Nuzzo, R.H. Friend, M.H. Song, Adv. Mater. 28 (2016) 6906–6913.
[8] M. Yuan, L.N. Quan, R. Comin, G. Walters, R. Sabatini, O. Voznyy, S. Hoogland, Y. Zhao, E.M. Beauregard, P. Kanjanaboos, Z. Lu, D.H. Kim, E.H. Sargent, Nat. Nanotechnol. 11 (2016) 872–877.
[9] N. Wang, L. Cheng, R. Ge, S. Zhang, Y. Miao, W. Zou, C. Yi, Y. Sun, Y. Cao, R. Yang, Y. Wei, Q. Guo, Y. Ke, M. Yu, Y. Jin, Y. Liu, Q. Ding, D. Di, L. Yang, G. Xing, H. Tian, C. Jin, F. Gao, R.H. Friend, J. Wang, W. Huang, Nat. Photonics 10 (2016) 699–704.
[10] Z. Xiao, R.A. Kerner, L. Zhao, N.L. Tran, K.M. Lee, T.-W. Koh, G.D. Scholes, B.P. Rand, Nat. Photonics 11 (2017) 108–115.
[11] F. Zhang, H. Zhong, C. Chen, X.-G. Wu, X. Hu, H. Huang, J. Han, B. Zou, Y. Dong, ACS Nano 9 (2015) 4533–4542.
[12] H. Huang, A.S. Susha, S.V. Kershaw, T.F. Hung, A.L. Rogach, Adv. Sci. 2 (2015) 1500194.
[13] J. Xing, F. Yan, Y. Zhao, S. Chen, H. Yu, Q. Zhang, R. Zeng, H.V. Demir, X. Sun, A. Huan, Q. Xiong, ACS Nano 10 (2016) 6623–6630.
[14] X. Zhao, N.-G. Park, Photonics 2 (2015) 1139–1151.
[15] M. Kulbak, S. Gupta, N. Kedem, I. Levine, T. Bendikov, G. Hodes, D. Cahan, J. Phys. Chem. Lett. 7 (2016) 167–172.
[16] J. Song, J. Li, X. Li, L. Xu, Y. Dong, H. Zeng, Adv. Mater. 27 (2015) 7162–7167.
[17] Q.V. Le, M. Park, W. Sohn, H.W. Jang, S.Y. Kim, Adv. Electron. Mater. 3 (2017) 1600448.
[18] G. Li, F.W.R. Rivarola, N.J.L.K. Davis, S. Bai, T.C. Jellicoe, F.D.L. Peña, S. Hou, C. Ducati, F. Gao, R.H. Friend, N.C. Greenham, Z.-K. Tan, Adv. Mater. 28 (2016) 3528–3534.
[19] L. Protesescu, S. Yakunin, M.I. Bodnarchuk, F. Krieg, R. Caputo, C.H. Hendon, R.X. Yang, A. Walsh, M.V. Kovalenko, Nano Lett. 15 (2015) 3692–3696.
[20] Q.A. Akkerman, V. D'Innocenzo, S. Accornero, A. Scarpellini, A. Petrozza, M. Prato, L. Manna, J. Am. Chem. Soc. 137 (2015) 10276–10281.
[21] X. Li, Y. Wu, S. Zhang, B. Cai, Y. Gu, J. Song, H. Zeng, Adv. Funct. Mater. 26 (2016) 2435–2445.
[22] F.C. Hanusch, E. Wiesenmayer, E. Mankel, A. Binek, P. Angloher, C. Fraunhofer, N. Giesbrecht, J.M. Feckl, W. Jaegermann, D. Johrendt, T. Bein, P. Docampo, J. Phys. Chem. Lett. 5 (2014) 2791–2795.
[23] A.A. Zhumekenov, M.I. Saidaminov, M.A. Haque, E. Alarousu, S.P. Sarmah, B. Murali, I. Dursun, X.-H. Miao, A.L. Abdelhady, T. Wu, O.F. Mohammed, O.M. Bakr, ACS Energy Lett. 1 (2016) 32–37.
[24] Y. Fu, H. Zhu, A.W. Schrader, D. Liang, Q. Ding, P. Joshi, L. Hwang, X.-Y. Zhu, S. Jin, Nano Lett. 16 (2016) 1000–1008.
[25] L. Protesescu, S. Yakunin, M.I. Bodnarchuk, F. Bertolotti, N. Masciocchi, A. Guagliardi, M.V. Kovalenko, J. Am. Chem. Soc. 138 (2016) 14202–14205.
[26] A. Perumal, S. Shendre, M. Li, Y.K.E. Tay, V.K. Sharma, S. Chen, Z. Wei, Q. Liu, Y. Gao, P.J.S. Buenconsejo, S.T. Tan, C.L. Gan, Q. Xiong, T.C. Sum, H.V. Demir, Sci. Rep. 6 (2016) 36733.
[27] J. Pan, L.N. Quan, Y. Zhao, W. Peng, B. Murali, S.P. Sarmah, M. Yuan, L. Sinatra, N.M. Alyami, J. Liu, E. Yassitepe, Z. Yang, O. Voznyy, R. Comin, M.N. Hedhili, O.F. Mohammed, Z.H. Lu, D.H. Kim, E.H. Sargent, O.M. Bakr, Adv. Mater. 28 (2016) 8718–8725.
[28] J. Li, L. Xu, T. Wang, J. Song, J. Chen, J. Xue, Y. Dong, B. Cai, Q. Shan, B. Han, H. Zeng, Adv. Mater. 29 (2017) 1603885.
[29] D. Battaglia, X. Peng, Nano Lett. 2 (2002) 1027–1030.
[30] Y. Liu, M. Gibbs, J. Puthussery, S. Gaik, R. Ihly, H.W. Hillhouse, M. Law, Nano Lett. 10 (2010) 1960–1969.
[31] T. Tachikawa, I. Karimata, Y. Kobori, J. Phys. Chem. Lett. 6 (2015) 3195–3201.
[32] D.W. Dequilettes, S.M. Vorpahl, S.D. Stranks, H. Nagaoka, G.E. Eperon, M.E. Ziffer, H.J. Snaith, D.S. Ginger, Science 348 (2015) 683–686.
[33] H. Huang, F. Zhao, L. Liu, F. Zhang, X.-G. Wu, L. Shi, B. Zou, Q. Pei, H. Zhong, ACS Appl. Mater. Interfaces 7 (2015) 28128–28133.
[34] D. Di, K.P. Musselman, G. Li, A. Sadhanala, Y. Ievskaya, Q. Song, Z.-K. Tan, M.L. Lai, J.L. MacManus-Driscoll, N.C. Greenham, R.H. Friend, J. Phys. Chem. Lett. 6 (2015) 446–450.
[35] K. Galkowski, A. Mitioglu, A. Miyata, P. Plochocka, O. Portugall, G.E. Eperon, J.T.-W. Wang, T. Stergiopoulos, S.D. Stranks, H.J. Snaith, R.J. Nicholas, Energy Environ. Sci. 9 (2016) 962–970.
[36] K. Wu, A. Bera, C. Ma, Y. Du, Y. Yang, L. Li, T. Wu, Phys. Chem. Chem. Phys. 16 (2014) 22476–22481.
[37] J. Chang, E.R. Waclawik, RSC Adv. 4 (2014) 23505–23527.
[38] Y.-H. Kim, C. Wolf, H. Cho, S.-H. Jeong, T.-W. Lee, Adv. Mater. 28 (2016) 734–741.
[39] H.-K. Seo, H. Kim, J. Lee, M.-H. Park, S.-H. Jeong, Y.-H. Kim, S.-J. Kwon, T.-H. Han, S. Yoo, T.-W. Lee, Adv. Mater. 29 (2017) 1605587.
[40] T.-H. Han, M.-R. Choi, S.-H. Woo, S.-Y. Min, C.-L. Lee, T.-W. Lee, Adv. Mater. 24 (2012) 1487–1493.
[41] T.-W. Lee, Y. Chung, O. Kwon, J.-J. Park, Adv. Funct. Mater. 17 (2007) 390–396.

Young-Hoon Kim received his M.S. (2014) in Division of Environmental Science and Engineering and Ph.D. (2016) in Material Science and Engineering from Pohang University of Science and Technology (POSTECH), Korea. He is currently working in Materials Science and Engineering at Seoul National University, Korea as a postdoctoral researcher (2016–2017). His research focuses on solution-processed electronics based on organic and organic-inorganic hybrid materials for flexible displays and solid-state lightings.

Geon-Hui Lee received his B.S. in Materials Science and Engineering from Pohang University of Science and Technology (POSTECH) in 2016. He is currently pursuing his integrated Ph.D. in Materials Science and Engineering at POSTECH. His research interests include nano-materials such as perovskite nanoparticles, black phosphorus nanoparticles and gold nanoparticles, and their application in bioelectronics.

Young-Tae Kim received his B.S. in Material Science and Engineering from Hanyang University in 2012. He is currently pursuing his Ph.D. in Material Science and Engineering at Pohang University of Science and Technology (POSTECH). His research interests include (1) quantitative and structural characterization of organic-based optoelectronic devices by transmission electron microscopy (TEM) and atom probe tomography (APT), (2) atomic scale analysis through the Cs-corrected TEM for nano-material and electronic devices, and (3) investigation of correlation between mico-structure and physical properties in electronic devices through in-situ electron microscopy.

Christoph Wolf received his B.S. and M.S. in Engineering Physics from University of Technology Graz, Austria. He is currently finishing his Ph.D. studies in the department of Materials Science and Engineering at Pohang University of Science and Technology (POSTECH). His studies focus on spectroscopy and first-principles calculation of novel semiconductor materials for opto-electronic applications.

Hyung Joong Yun is a senior researcher at Korea Basic Science Institute (KBSI). He received his B.S (2001) and M.S (2003) in Physics from University of Seoul. Before joining the KBSI, he was a researcher at Samsung Advanced Institute of Technology (SAIT). He received Ph.D in Semiconductor and Chemical Engineering from Jeonbuk National University in 2017. His research interests include analysis of surface and interface structure in OPVs, using X-ray/UV photoelectron spectroscopy and other techniques. His current research focuses on the study of catalytic reaction at the gas-solid interfaces by in-situ ambient pressure X-ray photoelectron spectroscopy (AP-XPS).

Woosung Kwon received his B.S. in Chemical Engineering with a minor in Physics (2010) and Ph.D. in Chemical Engineering (2013) from Pohang University of Science and Technology (POSTECH). After postdoctoral research at Stanford University, he joined the faculty of Sookmyung Women's University, where he is now serving as an assistant professor of chemical and biological engineering. His research interests include (1) development of functional, biocompatible nanomaterials for theragnostic and optoelectronic applications, (2) advancement of functionality of nanomaterials through atomic doping and molecular conjugation, and (3) study of the effect of nanomaterials on physiological biochemical processes in living organisms to address nanotoxicological issues.

Chan Gyung Park received his Ph.D. in Material Science and Engineering from Northwestern University in 1983. After three years of staff scientist at Oak Ridge National Laboratory, he joined the faculty of Pohang University of Science and Technology (POSTECH) in 1986. He is currently a professor in the Department of Material Science and Engineering at POSTECH and a director for National Institute for Nanotechnology (NINT) in Pohang. His current research interests are nanoscale HREM analyses microscopic phase transformation studies of advanced high-strength low alloy steels, and in-situ straining TEM analysis of super plastic deformation.

Tae-Woo Lee is an associate professor in Materials Science and Engineering at Seoul National University, Korea. He received his Ph.D in Chemical Engineering from KAIST, Korea in 2002. He joined Bell Laboratories, USA as a postdoctoral researcher and worked in Samsung Advanced Institute of Technology as a member of research staff (2003–2008). He was an associate professor in Materials Science and Engineering at Pohang University of Science and Technology (POSTECH), Korea until Aug, 2016. His research focuses on printed electronics based on organic and organic-inorganic hybrid materials for flexible displays, solid-state lightings, and solar-energy-conversion devices.